# A biophysical, minimal model to investigate age-related changes in CA1 pyramidal cell excitability

Erin C. McKiernan[1*], Marco A. Herrera-Valdez[2**], and Diano F. Marrone[3,4]

[1]Departamento de Física, Facultad de Ciencias, Universidad Nacional Autónoma de México
[2]Laboratorio de Fisiología de Sistemas, Departamento de Matemáticas, Facultad de Ciencias, Universidad Nacional Autónoma de México
[3]McKnight Brain Institute, University of Arizona
[4]Department of Psychology, Wilfrid Laurier University
[*]Corresponding author: emckiernan@ciencias.unam.mx
[**]Corresponding author: marcoh@ciencias.unam.mx

May 14, 2020

**Abstract**

Aging is a physiological process that is still poorly understood, especially with respect to effects on the brain. There are open questions about aging that are difficult to answer with an experimental approach. Underlying challenges include the difficulty of recording *in vivo* single cell and network activity simultaneously with submillisecond resolution, and brain compensatory mechanisms triggered by genetic, pharmacologic, or behavioral manipulations. Mathematical modeling can help address some of these questions by allowing us to fix parameters that cannot be controlled experimentally and investigate neural excitability under different conditions. Previous modeling approaches in the CA1 region of the hippocampus have provided many insights, but have also been limited by an inherent trade-off between physiological accuracy and computational load. Herein, we present a biophysical, minimal model of CA1 pyramidal cells (PCs) based on equations derived from first principles of thermodynamics. The model allows directly varying the contribution of transmembrane transport proteins by changing their number. By analysing the dynamics of the model we find parameter ranges that reproduce both the variability in electrical activity seen in young and adult PCs. In particular, the model explains the dynamics underlying age-related changes in excitability that are qualitatively and quantitatively similar to those observed in aging PCs, as caused by increased L-type $Ca^{2+}$ channel expression.

## 1 Introduction

As we age, our brains undergo many changes [1–3], but we understand relatively little about these and their effects on neural function. What does normal neurophysiological aging look like and what are the various stages? How do the biophysical properties and the electrical activity of neurons

change during aging? How do aging neurons respond to input from other cells? Answering these questions is not just fundamental to understanding aging as a neurophysiological process, but also to understanding how this process may be altered in age-related disorders of clinical importance such as Alzheimer's and Parkinson's disease.

Many aging studies have focused on the hippocampus, an area of the brain involved in learning, memory formation, and spatial processing [1–3]. Aged rats [4–9] and humans [10, 11] show impaired learning of hippocampal-dependent spatial tasks. Long-term potentiation (LTP), a proposed physiological substrate of memory formation, has been investigated in the hippocampus and its induction and maintenance shown to be impaired in aged rats [4, 8, 12, 13]. A short-term form of plasticity, frequency potentiation/facilitation (FP/FF), is also impaired in hippocampal pyramidal cells (PCs) from aged rats and correlates with learning deficits [14, 15].

Plasticity changes and behavioral impairments may result in part from altered excitability and disrupted $Ca^{2+}$ regulation in aged neurons [1–3]. CA1 PCs from aged animals show larger and longer post-burst afterhyperpolarizations (AHPs) [16–20]. AHPs are mediated by $Ca^{2+}$-dependent $K^+$ currents, which can act like brakes on the electrical activity of CA1 PCs [21, 22]. As a result, PCs show increased spike frequency adaptation and fire fewer action potentials (APs) in response to acute stimuli or during bursting activity [23–25]. Larger AHPs are associated with increased intracellular $Ca^{2+}$, mediated in part by $Ca^{2+}$ entry via L-type channels [20, 24, 26–28]. Aged animals show increases in L-type channel expression and/or channel density at the plasma membrane [29–33]. Animals with higher $Ca^{2+}$ channel density perform poorly in spatial tasks [30], while blockers of L-type $Ca^{2+}$ channels can restore learning and plasticity in older animals [34–36].

Despite extensive study, it is still not well understood how changes in ion channel gene expression and hippocampal PC excitability may affect neuron responsiveness and microcircuit output. In part, this is due to challenges inherent to performing the needed experiments, especially in mammalian systems. Single PCs are difficult to access in intact animals where hippocampal microcircuit function is preserved. In addition, it is difficult to tease apart the influence of each the many different neurophysiological factors that change during aging. Mathematical modeling provides means to understand more about the effects of aging on hippocampal cellular excitability by performing manipulations that are not possible to implement in experiments.

Several mathematical models have been constructed to investigate electrical activity in CA1 PCs [37–42]. Some include representations of PC morphology using multiple compartments [39–42], making mathematical analysis difficult and increasing computational load. Single-compartment models of CA1 PCs exist, but include numerous ionic currents (up to 10) and 5 or more variables [37, 38]. As the number of variables increases, analysis becomes harder and limits our ability to understand the influence of specific parameters, as well as complicating the construction of simple network models. Finally, the existing model formulations are conductance-based (e.g. Hodgkin-Huxley type [43]), which only takes into account linear approximations of the fluxes that make up the transmembrane currents [44]. Our previous work shows that mathematical expressions for ionic currents for different passive and active transport mechanisms can be derived from first principles of thermodynamics [44–46], using a common functional form. This results in a more realistic representation of ionic flow across the membrane, and allows the model to reproduce phenomena such as rectification of ion currents observed in recordings but not reproduced by

conductance-based models.

We present a model that reproduces the diversity of firing patterns seen in CA1 PC recordings, including repetitive slow firing with frequency adaptation, stimulus-induced bursting, and spontaneous bursting [47]. We do so by studying families of 3-dimensional dynamical systems with a common formulation (same functional form describing the dynamics), based on basic biophysical descriptions. In addition, we reproduce several electrophysiological characteristics of aging simply by varying the expression of $Ca^{2+}$ channels in the model membrane, and make predictions about differences in bursting activity in aged cells, which to our knowledge has not yet been reported. We argue this model is ideal to further study the effects of different biophysical changes in CA1 PCs during aging, as well as potentially forming the basis for biophysical, yet computationally inexpensive network models.

# 2 Methods

## 2.1 Model

To simulate the electrical activity of CA PCs, we used an extended version of a two-dimensional, biophysical model previously developed and characterized by two of the present authors (ECM and MAHV) [44–46]. The equations for the ionic currents are derived from first principles of thermodynamics. The advantages of the model over previous conductance-based formulations are: (1) a representation of ionic currents using biophysical principles that includes rectification as observed in electrophysiological recordings; (2) each parameter in the model corresponds to a measurable experimental quantity, meaning we can easily incorporate data, as well as make testable physiological predictions; and (3) our model formulation allows us to vary the number of specific ion channels in the membrane. In other words, the model allows us to simulate functional changes in gene expression.

Previous modeling studies have shown that to reproduce firing behaviors such as spike frequency adaptation and bursting, the minimum number of variables is three [48, 49]. In particular, $Ca^{2+}$ dynamics are important for producing adaptation and burst firing in CA1 PCs (for review see [47]). Therefore, we extended our previous model to include $Ca^{2+}$ dynamics, $Ca^{2+}$ currents, and $Ca^{2+}$-currents gated by $Ca^{2+}$.

The model dynamics are given by three ordinary differential equations that describe the time-dependent changes of $v$, $w$, and $c$, respectively representing the transmembrane potential, the proportion of open delayed rectifier $K^+$ channels, and the intracellular $Ca^{2+}$ concentration [44]. sout(dot notation represents the derivative with respect to time)

The change in the membrane potential is the sum of the transmembrane ionic fluxes normalized by the membrane capacitance. Explicitly,

$$C_m \partial_t v = I_F - I_{NaT}(v, w) - I_{CaL}(v, c) - I_{DK}(v, w) - I_{SK}(v, c) - I_{NaK}(v), \tag{1}$$

[mh]Here $\partial_t G$ represents the instantaneous change in G with respect to time. $C_m$ (pF) is a constant representing the change in charge around the membrane with respect to the membrane potential typically referred to as membrane capacitance in conductance-based models, [50]). The term

$I_F$ represents a stimulus *forcing* the membrane either by incoming current from an electrode, or from the local field potential (simulations of spontaneous activity). The fluxes in quation (1) are all given by the product of an amplitude term (pA), a gating term, a flux driving force (Table 1). The amplitude terms $a_x$ are given by $s_x N_x$. The term $s_x$ (pA) is the current flowing through a single transmembrane protein (typically around 1 pA for most voltage-gated channels [51]), and $N_x$ is the number of membrane proteins mediating the current (e.g. number of $K^+$channels). In our calculations and estimations of the contributions of the different ion fluxes to the change in $v$, we use $a_x = s_x N_x$ (pA) as an approximation for the whole-cell current. The flux across the membrane mediated by the different transmembrane transport mechanisms represented in the model is given by

$$F_x(v) = \exp\left(b_x g_x \frac{v - v_x}{v_T}\right) - \exp\left((b_x - 1) g_x \frac{v - v_x}{v_T}\right), \quad x \in \{N, C, K, NK\} \tag{2}$$

The term $b_x$ in (2) represents the transport bias across the membrane in either direction for a given ion channel or pump (b = 0.5 means transmembrane transport is bidirectional and symmetrical, i.e. no rectification, which means assymetrical ion flux [44]). The thermal potential $v_T = kT/q$ (mV), where $k$ is Boltzmann's constant (mJ/$^o$K), $T$ is absolute temperature ($^o$K), and $q$ is elementary charge (Coulombs). The Boltzmann constant can be thought of as a scaling factor between macroscopic (thermodynamic temperature) and microscopic (thermal energy) physics [52]. The Nernst potential for each ion $x$ ($Na^+$, $Ca^{2+}$, or $K^+$) is given by:

$$v_x = \frac{v_T}{z_x} \ln\left(\frac{[x]_o}{[x]_i}\right) \tag{3}$$

where $z_x$ is the ion valence and $[x]_o$ and $[x]_o$ represent concentrations outside and inside the cell, respectively. The reversal potential for the Na-K ATPase is given by $v_{NaK} = 3v_{Na} - 2v_K - v_{ATP}$ [44].

**Table 1:** All ion fluxes are given by a product of the form $I_x = a_x G_x F_x$ where $a_x$, $G_x$, and $F_x$ represent, respectively, the amplitude (normalized by membrane capacitance), gating, and driving force terms for the flux. The gating term for the $Na^+$-$K^+$pump can be written as 1, which can be thought of as saturation. Note that the inactivation of $Na^+$-channels is also represented by $w$ [53, 54]. The proportion of non-inactivated $Na^+$channels is thus $1 - w$.

| Mechanism | Name | Amplitude ($a$) | Gating ($G$) | Flux $F$ |
|---|---|---|---|---|
| Transient Na current | $I_{NaT}(v, w)$ | $a_{Na}$ | $S_m(v)(1 - w)$ | $F_{Na}(v)$ |
| L-type $Ca^{2+}$ current | $I_{CaL}(v, c)$ | $a_{Ca}$ | $S_n(v)$ | $F_{Ca}(v)$ |
| Delayed rectifier $K^+$ channel | $I_{DK}(v, w)$ | $a_{DK}$ | $w$ | $F_K(v)$ |
| SK $Ca^{2+}$-dependent $K^+$ channel | $I_{SK}(v, c)$ | $a_{SK}$ | $H_{SK}(c)$ | $F_K(v)$ |
| $Na^+$-$K^+$ pump | $I_{NaK}(v)$ | $a_{NaK}$ | 1 | $F_{NaK}(v)$ |

**Gating.** The dynamics for $w$, the proportion of activated delayed-rectifier $K^+$channels, are assumed to be logistic,

$$\partial_t w = r_w w(S_w(v) - w)R_w(v), \tag{4}$$

which yields better fits, and is more consistent with, the dynamics of activation in channel populations recorded in voltage-clamp experiments [43, 55, 56]. The parameter $r_w$ is the recovery rate for $w$ toward its voltage-dependent steady state $S_w(v)$. The function $R_w$ describes the voltage-dependence of the rate of activation of the channels.

The auxiliary functions for voltage-dependent gating are given by

$$S_j(v) = \frac{\exp\left(g_j \frac{v-v_j}{v_T}\right)}{1 + \exp\left(g_j \frac{v-v_j}{v_T}\right)}, \quad j \in \{m, n, w\} \tag{5}$$

$$R_j(v) = \exp\left(b_j g_j \frac{v - v_j}{v_T}\right) + \exp\left((b_j - 1) g_j \frac{v - v_j}{v_T}\right) \tag{6}$$

where $g_j$ represents the steepness of the activation curve for $Na^+(m)$, $Ca^{2+}(n)$, or $K^+(w)$ channels; $v_j$ represents the half-activation voltage for those channels, and $b_j$ in (6) represents the assymetry in the gating relative to voltage that biases the time constant for the gating process.

The gating of the SK channel is not voltage-dependent. Instead, it depends on intracellular $Ca^{2+}$- binding, its activation is modeled using a Hill equation that depends on the intracellular concentration of $Ca^{2+}$, as used to fit data from channel recordings [57]:

$$G_{SK}(c) = \frac{c^2}{c^2 + c_{SK}^2} \tag{7}$$

where $c_{SK}$ represents the half-activation $Ca^{2+}$concentration for the $Ca^{2+}$-dependent $K^+$-channels.

For the dynamics of intracellular $Ca^{2+}$we assume recovery toward a steady state $c_\infty$ at a rate $r_c$, with increments caused by the $Ca^{2+}$current $J_{Ca}$.

$$\partial_t c = r_c(c_\infty - c) - k_c J_{CaL}(v, c). \tag{8}$$

The term $k_c$ in equation (8) is the conversion factor that accounts for the effect of $Ca^{2+}$flux across the membrane on the intracellular$Ca^{2+}$concentration.

Spontaneous activity is simulated by replacing the term $J_F$ with a time-dependent, Ornstein-Uhlenbeck (OU) process with amplitude $a_F(t)$ (pA). The mean is represented by $\mu_F$ (pA) (drift term) [58] given by [59, 60]

$$a_F(t + \delta) \;=\; a_F(t)\left(1 - \frac{\delta}{\tau_F}\right) + \left[\mu_F \delta + \eta(t)\sqrt{d_{Stim}\delta}\right], \tag{9}$$

where $\delta$ is a small time step, $\tau_F$ is a relaxation time, $\eta(t)$ is an independent white noise process with zero-mean and unit standard deviation. The process has a variance $\sigma_F^2 = d_F\delta/2$ (pA), which means that $d_F$ can be approximated if an estimation of the variance of the current $a_F$ is available [61, 62].

**Change of variables to obtain numerical solutions.** To simplify the numerics, we change variables

$$y = v/v_T,$$

and adjust all voltages accordingly as

$$y_l = v_l/v_T.$$

The new equation for the normalized voltage is

$$\partial_t y = \frac{\partial_t v}{v_T}$$

. To simplify the notation and reduce the number of operations during the numerical integration, we also reparametrize the amplitudes as

$$A_l = \frac{a_l}{v_T\, Cm}.$$

in units of 1/ms. The result is a new equation of the form

$$\begin{aligned} \partial_t y &= J_F - A_{NaKa} F_{NaKa}(y) && (10)\\ &\quad - \left( A_{KaD} w + A_{KaSK} \frac{^2}{c^2 + c_0^2} \right) F_K(y) && (11)\\ &\quad - A_{NaT}(1-w) m_\infty(y) F_{Na}(y) - A_{CaL} m_{13\infty}(y) F_{Ca}(y,c), && (12) \end{aligned}$$

with driving force terms of the form

$$F_l(y) = 2\sinh\left(\frac{y - y_l}{2}\right),$$

for $l \in \{NaKa, KaD, KaSK, NaT, CaL\}$. The term $J_F$ (1/ms) is the input current $I_F$ (pA) divided by $v_T C_m$.

## 2.2 Parameters

The ionic currents were modeled to fit as closely as possible the biophysical properties of those carried by channel variants expressed in mammalian neurons, and specifically CA1 PCs, where data are available. For example, the DK current is based on that mediated by $K_v2.1$ channels, found to be the predominant channel underlying the delayed rectifier current in rat hippocampal neurons [63]. The L-type $Ca^{2+}$ current is based on that carried by $Ca_v1.2$ (class C) channels, found to be the predominant L-type channel isoform expressed in rat brain [64]. Additional details about the model current parameters can be found in Table 2.

Wherever possible, model parameters were taken from studies in rodent (mice and rat) hippocampal CA1 PCs. If data were not available, we obtained parameters from other types of mammalian cell, or from studies of mammalian ion channels in expression systems like *Xenopus* oocyte. Physical constants and other parameters which we would not expect to vary, such as the intra- and extracellular concentrations of ions or the cellular capacitance, were fixed. Biophysical properties of

the ion channels, such as their half-activation voltages, were also fixed. The parameters we varied were primarily those corresponding to maximum current amplitudes, which can change acutely due to modulation or channel phosphorylation [65, 66], or chronically due to changes in ion channel expression that occur with age [29, 31, 67].

**Table 2:** Constants and parameters. Note $v_{NaK} = 3v_{Na} - 2v_K - v_{ATP}$.

| parameter | description | value | units | reference |
|---|---|---|---|---|
| $k$ | Boltzmann's constant | 1.381e$^{-20}$ | mJ/K | physical constant [51] |
| $q$ | elementary charge | 1.602e$^{-19}$ | C | physical constant [51] |
| $T$ | absolute temperature | 273.15 + 37 | K | adjusted to mammalian body temperature of 37℃ [51] |
| $C_m$ | membrane capacitance | 25.0 | pF | in range reported in rat CA1 PCs [68] |
| $a_{NaT}$ | amplitude of transient $Na^+$ current | 1.5-3.5 | pA | set to produce currents of ∼3-7 nA as recorded in CA1 PCs from rats [69] and guinea pigs [70] |
| $a_{CaL}$ | amplitude of L-type $Ca^{2+}$ current | 0.4 or 0.7 | pA | set to produce currents of ∼2-3 nA or ∼5-6 nA as recorded in young and aged CA1 PCs, respectively [26] |
| $a_{DK}$ | amplitude of delayed rectifier $K^+$ current | 20-50 | pA | set to produce currents of ∼7-10 nA as recorded from HEK cells expressing rat Kv2.1 and $J_K$ in hippocampal neurons [71] |
| $a_{SK}$ | amplitude of $Ca^{2+}$-dependent $K^+$ current | 1.1-2.5 | pA | set to produce currents of ∼300 pA to 1.2 nA, depending on $Ca^{2+}$ concentration, as recorded in SK-transfected cells [72] |
| $a_{NaK}$ | amplitude of $Na^+/K^+$ ATPase current | 0.015-0.035 | pA | set to produce currents of ∼90-250 pA, similar to but on high end of range recorded in hippocampal PCs [73] |
| $v_{Na}$ | Nernst potential for $Na^+$ | 65 | mV | in range reported for mammalian cells [74] |
| $v_{Ca}$ | Nernst potential for $Ca^{2+}$ | variable; baseline 135 | mV | in range reported for mammalian cells [74] |
| $v_K$ | Nernst potential for $K^+$ | -89 | mV | in range reported for mammalian cells [74] |
| $v_{ATP}$ | Nernst potential for ATP | -450 | mV | value used in model of mammalian heart cells and based on fit to data [75] |
| $v_{NaK}$ | Nernst potential for $Na^+/K^+$ ATPase | -76 | mV | calculated based on the Nernst potentials for ATP, $Na^+$, and $K^+$, and a 3:2 stoichiometry, respectively [76] |
| $r_w$ | rate of activation of delayed rectifier $K^+$ current | 1.0-2.5 | ms | in range recorded from CA1 PCs in slice [77] or hippocampal neurons in culture [78] |
| $s_m$ | symmetry of time constant of transient $Na^+$ current | 0.5 | - | based on voltage dependence of time constant recorded in rat CA1 PCs [79] |
| $s_n$ | symmetry of time constant of L-type $Ca^{2+}$ current | 0.5 | - | based on voltage dependence of time constant recorded in guinea pig CA1 PCs [80] |

| parameter | description | value | units | reference |
|---|---|---|---|---|
| $s_w$ | symmetry of time constant of delayed rectifier $K^+$ current | 0.3 | - | based on fit; if higher (0.5-0.7) APs are the wrong shape and do not ride on sufficient plateau potential compared to recordings |
| $v_m$ | half-activation potential of $Na^+$ current | -19 | mV | in range reported for transient $Na^+$ channels in CA1 PCs [79, 81, 82] |
| $v_w$ | half-activation potential of delayed rectifier $K^+$ current | -1 | mV | in range reported for rat Kv2.1 channels expressed in COS-1 cells [63] |
| $v_n$ | half-activation potential of L-type $Ca^{2+}$ current | 3 | mV | in range recorded for high-voltage activated $Ca^{2+}$ currents in rat CA1 PCs [83]; see also recordings from oocytes [84] or HEK cells [85] expressing $Ca_v1.2$ channels |
| $c_{SK}$ | half-activation $Ca^{2+}$ concentration for SK current | 740 | nM | based on recordings from oocytes expressing rat SK channel variant [86] |
| $z_m$ | activation slope of transient $Na^+$ current | 4.0 | - | |
| $g_n$ | activation slope of L-type $Ca^{2+}$ current | 4.0 | - | |
| $g_w$ | activation slope of delayed rectifier $K^+$ current | 4.0 | - | fit to data from rat brain delayed rectifier channels [87] |
| $c_\infty$ | minimum intracellular $Ca^{2+}$ concentration | 100 | nM | approximate resting intracellular $Ca^{2+}$ concentration reported in rat CA1 PCs [23, 88, 89] |
| $r_c$ | $Ca^{2+}$ removal rate constant | $8e^{-3}$ to $1e^{-3}$ | - | adjusted to produce $Ca^{2+}$ dynamics as recorded in rat CA1 PCs [88] |
| $k_c$ | $Ca^{2+}$ current to concentration conversion factor | $8e^{-6}$ to $6e^{-6}$ | - | adjusted to produce $Ca^{2+}$ dynamics as recorded in rat CA1 PCs [88] |

By exploring the model through parameter variations, we were able to find parameter sets that produced different firing patterns, such as adaptive firing, conditional bursting, and spontaneous bursting. These firing patterns are described in more detail in the Results section, but the respective parameter sets are included in Table 3 for ease of comparison.

## 2.3 Simulations

All code was written in Python 2.7 and run on MacBook Pro laptops with 2.9 GHz Intel Core i5 processors. Simulations were performed using functions from the Python library SciPy [90]. All figures were produced with the Python library Matplotlib [91]. OU processes were simulated using the pyprocess module [92].

**Table 3:** Parameters used to produce different firing patterns in the yPC model. The normalization of amplitudes was calculated with $v_T C_m = 668.171$ mv pF. Amplitudes in pA are included (in parentheses) for reference with respect to experimental measures.The amplitude for the L-type $Ca^{2+}$current in the aPC was set to $a_{CaL}$=467.719 pA, which is equivalent to $A_{CaL}$=0.7 (1/ms)

| parameter | adaptive firing | conditional bursting | spontaneous bursting |
|---|---|---|---|
| $A_{NaK}$ ($a_{NaK}$ pA) | 0.015 (10.0226) | 0.020 (13.3634) | 0.040 (26.7268) |
| $A_{KD}$ ($a_{KD}$ pA) | 40.0 (26726.8) | 20.0 (13363.4) | 30.0 (20045.1) |
| $A_{SK}$ ($a_{SK}$ pA) | 1.1 (734.988) | 2.5 (1670.43) | 1.1 (734.988) |
| $A_{Na}$ ($a_{Na}$ pA) | 1.5 (1002.26) | 2.0 (1336.34) | 4.0 (2672.68) |
| $A_{CaL}$ ($a_{CaL}$ pA) | 0.4 (267.268) | 0.4 (267.268) | 0.4 (267.268) |
| $r_{KD}$ | 1.0 | 2.5 | 1.0 |
| $r_{Ca}$ | $1e^{-3}$ | $5e^{-3}$ | $1e^{-2}$ |
| $k_{Ca}$ | $8e^{-6}$ | $6e^{-6}$ | $6e^{-6}$ |

## 2.4 Code availability

All Python code from this study is available via GitHub (https://github.com/emckiernan/agingCA1) and shared under the MIT license (https://opensource.org/licenses/MIT) to facilitate reuse. To promote reproducibility, we included a Jupyter notebook [93, 94] in the repository that explains how to use the code and generate the figures presented here.

## 2.5 Study design

While aged cells display a number of biophysical changes, we focused on their $Ca^{2+}$ channel expression. Aged CA1 PCs show an increase in the number of functional transmembrane L-type $Ca^{2+}$ channels [29–32, 95]. In particular, CA1 PCs from aged rats have increased expression of Cav1.2 at the plasma membrane [33]. With these results in mind, we decided to simulate aging by changing the number of Cav1.2 channels in our model membrane. We asked the question, is a change in Cav1.2 expression sufficient to reproduce the various changes in excitability, such as increased spike frequency adaptation, observed experimentally in aged CA1 PCs? In addition, CA1 PCs are known to burst [47], but we are not aware of any studies comparing the bursting patterns of young versus aged animal cells. Therefore, we used our model to further investigate the effects of altered Cav1.2 channel density on bursting activity. In all the following simulations, young and aged model PCs are identical with respect to every parameter except the maximum amplitude of their L-type $Ca^{2+}$ current, which is set to produce currents of $\sim$2-3nA or $\sim$5-6nA to match the magnitude of currents seen in recordings from young and aged animal CA1 PCs, respectively [26].

The PC models for young and old animals will be refered to as yPC and aPC respectively.

# 3 Results

CA1 PCs display diverse firing patterns, ranging from repetitive spiking with frequency adaptation to stimulus-induced, or even spontaneous, bursting (for review see [47]). Thus, to accurately represent these cells, our model must reproduce this diversity of firing as well as age-related effects on firing already reported in the literature.

## 3.1 Modeling age-related changes in spike frequency adaptation

Many CA1 PCs respond to square-pulse current injection by firing several early spikes followed by marked adaptation which slows the frequency of firing [23, 96–102]. Therefore, our first challenge was to tune the model to produce an adaptive firing pattern. We set the ionic currents to be the same amplitude range as observed in patch recordings of adult CA1 PCs, with amplitudes for the $Na^+$ and $Ca^{2+}$ currents or approximately 3 nA, for the DK current approximately double the inward cationic currents, and small for the SK current, between 250 pA to just over 1 nA, depending on the intracellular $Ca^{2+}$ concentration (see Table 2 for more details and references). This balance of ionic currents successfully reproduces adaptive firing seen in young adult PCs (Fig. 1, left column).

Recordings show that spike frequency adaptation is more pronounced in aged than in young animals, leading to a shorter initial period of fast spiking, followed by fewer spikes or even complete cessation of firing [23–25, 103]. Stronger adaptation in aPCs may be relevant to circuit function, as it is correlated with learning impairment [25, 103]. To compare the yPC and aPC models, all parameters were fixed except for the maximum amplitude of the L-type $Ca^{2+}$ current, which was set to produce currents of $\sim$2-3 nA (young) or $\sim$5-6 nA (old), based on recordings [26]. This difference in the $Ca^{2+}$ current is sufficient to reproduce the change in adaptation seen in yPC versus aPCs. Increased $Ca^{2+}$ channel density in the aPC model causes the number of spikes fired in the first 100 ms after stimulus onset to decrease from 6 to 4 spikes, and further slows firing for the remaining period of current injection (Fig. 1, right column). These results are similar to those found in recordings of CA1 PCs in young and old rabbits [24].

Comparing the ionic currents produced in each PC model during individual APs (Fig. 1, third and fourth rows) we see that the $Na^+$ currents are equivalent in the two cells but the $Ca^{2+}$ current in the aPC is approximately double that in the yPC, as expected with our parameter settings. Interestingly, despite setting the delayed rectifier $K^+$ channel expression to be the same in the two cells, $I_{KD}$ was larger in aPC by $\sim$2 nA. This increased $I_{KD}$ appears to be a consequence of the larger depolarization produced in the aPC model due to increased $Ca^{2+}$ influx. The APs in aPC are $\sim$3-4 mV larger than those in the yPC model, which increases the driving force for $K^+$ entry. However, increased $I_{KD}$ is not responsible for the stronger adaptation in aPC, as this current decreases rather than increases as firing proceeds. Furthermore, scaling the KD current back down in aged cells to compensate does not recover the firing pattern seen in young animal cells. These results are not shown here, but can be confirmed by running the simulations within our Jupyter notebook (github.com/emckiernan/agingCA1).

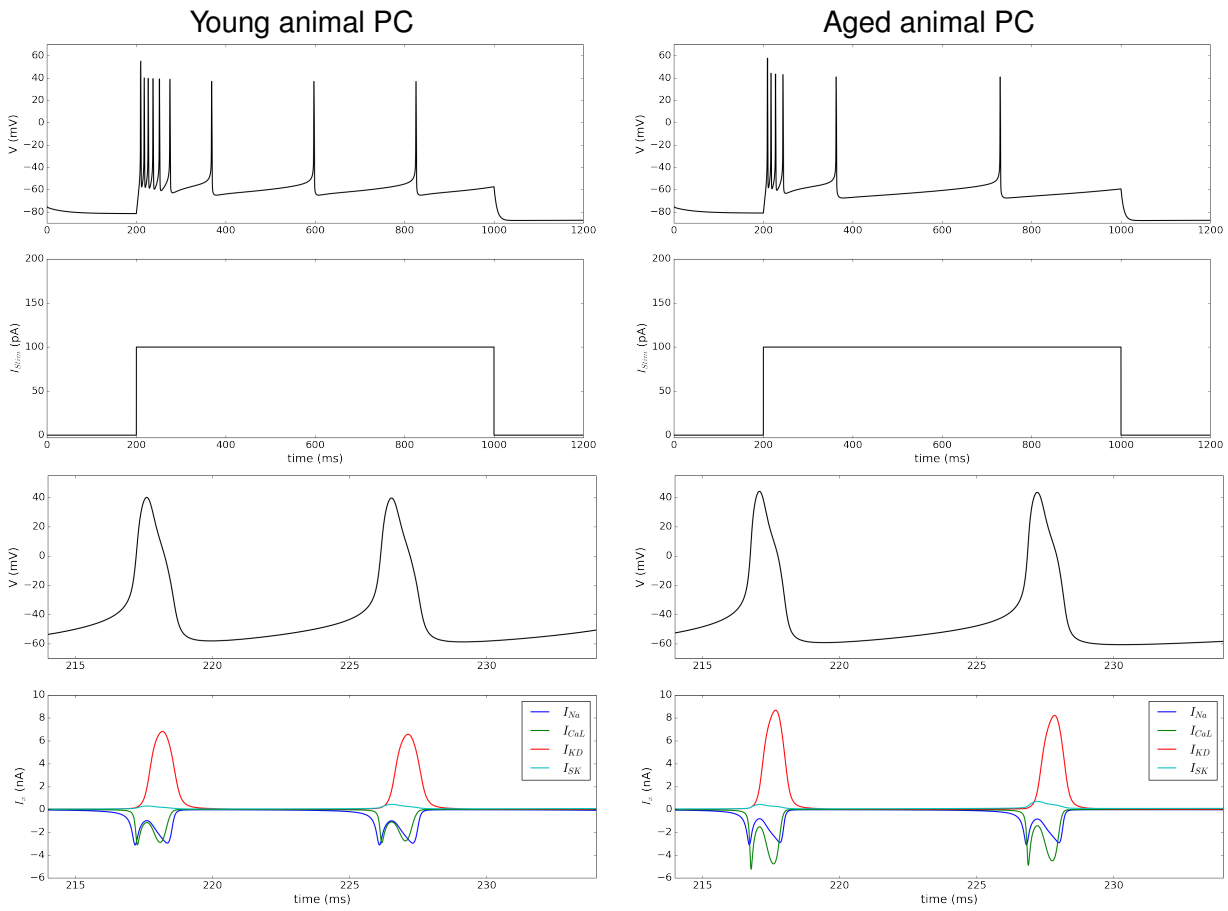


**Figure 1:** Responses of yPC (left column) and aPCs (right column) models to an 800 ms 100 pA square pulse current injection. The top row shows the voltage responses of each cell to the stimulus shown in the second row. The third row zooms in on two APs fired early in the response to better visualize their time course and amplitude, while the fourth row shows the amplitude and dynamics of the corresponding ionic currents. Parameters for yPC: $A_{NaT}$ = 1.5, $A_{CaL}$ = 0.4, $A_{KaD}$ = 40.0, $A_{KaSK}$ = 1.1, $r_{KaD}$ = 1.0, $r_{Ca}$ = 1e$^{-3}$, $k_{Ca}$ = 8e$^{-6}$. All parameters for aPC the same except $A_{CaL}$ = 0.7.

Examining the voltage response and the $Ca^{2+}$ and SK currents generated in the first 100 ms after stimulus onset reveals the mechanisms underlying the stronger adaptation in the aPC model (Fig. 2). The larger $Ca^{2+}$ current causes aPC to fire sooner after stimulus onset, which initially appears as a form of increased excitability. However, over time, the larger increase in intracellular $Ca^{2+}$ in turn produces a larger $Ca^{2+}$-dependent SK current, which slows firing to a greater extent in the aPC. While the first two spikes occur earlier in the aPC versus yPC, this temporal relationship flips by the third spike (Fig. 2, top panel), when the yPC model begins to spike sooner. By the fourth spike, activity in the aPC is significantly delayed with respect to the yPC. The aPC fails to spike again in this time period, while the yPC fires two more times. Closer inspection of the voltage traces, especially following the fourth spike in the aPC, shows a prolonged AHP that prevents the aPC from firing.

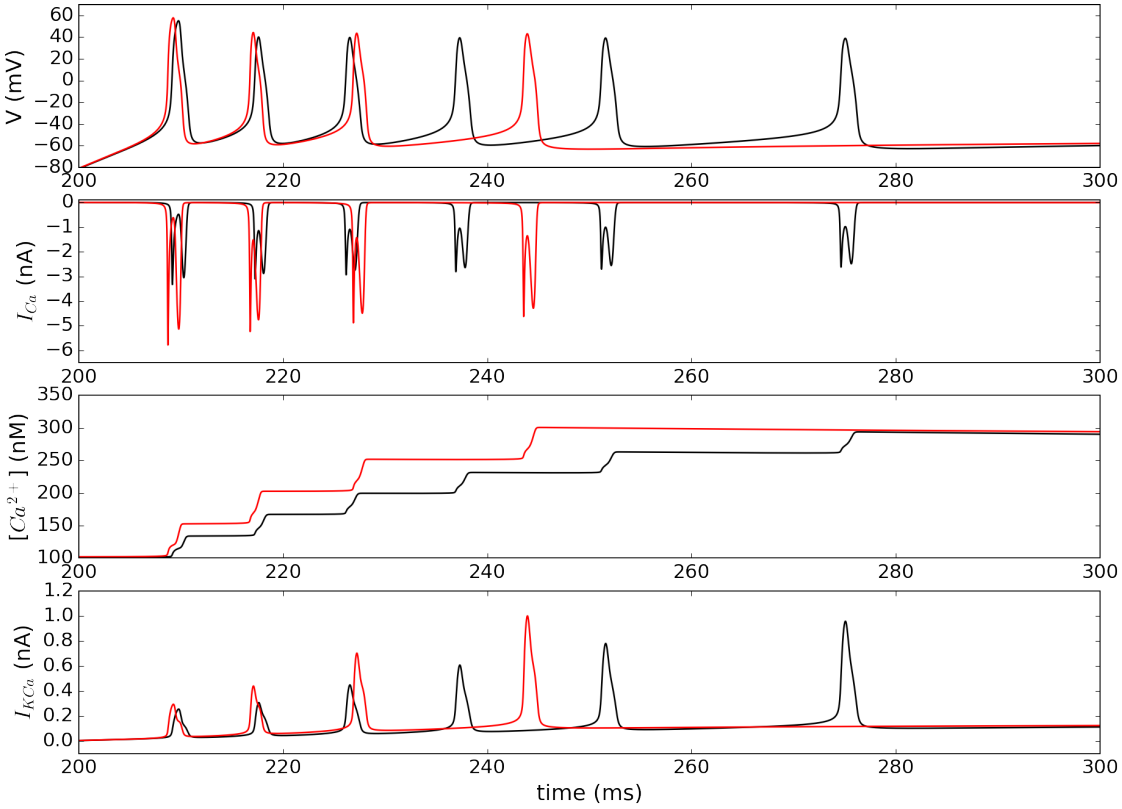


**Figure 2:** Spike frequency adaptation in the yPC (black traces) versus aPC (red traces) models. First ∼100 ms of voltage responses (top panel) shown in Fig. 1. Corresponding $Ca^{2+}$ currents, intracellular $Ca^{2+}$ concentration, and SK currents for each cell can be seen in the second, third, and fourth panels, respectively.

## 3.2 Modeling age-related changes in AHPs

AHP generation has been studied in CA1 PCs [39, 104, 105], particularly in the context of aging and excitability [19, 20, 23, 24, 103, 106–109]. To induce AHPs, we made small to moderate increases to the $Na^{+}$, KD, and SK maximum current amplitudes, while staying within the physiological ranges reported in the literature. We then stimulated model neurons with a 100 ms square pulse of sufficient amplitude to generate a burst of 5 action potentials (Fig. 3). The AHPs produced under these conditions in the yPC model had a peak amplitude of ∼6 mV, similar to recordings [20, 109, 110].

The aPCs model required more current than the yPC model to fire the same number of spikes (120 vs. 80 pA), suggesting that the aPC model is less excitable. However, as seen in previous simulations, aPC fires earlier than yPC due to its increased $Ca^{2+}$ current (Fig. 3, top panel inset). The aPC model generates an AHP ∼1 mV larger than seen in the yPC model (Fig. 3, second panel), similar to the magnitude of the difference observed in recordings [20, 23, 24, 107]. In the model, this larger AHP is due to an increased accumulation of $Ca^{2+}$ in the aged cell, which in turn produces a larger $SK$ current (Fig. 3, third and fourth panels).

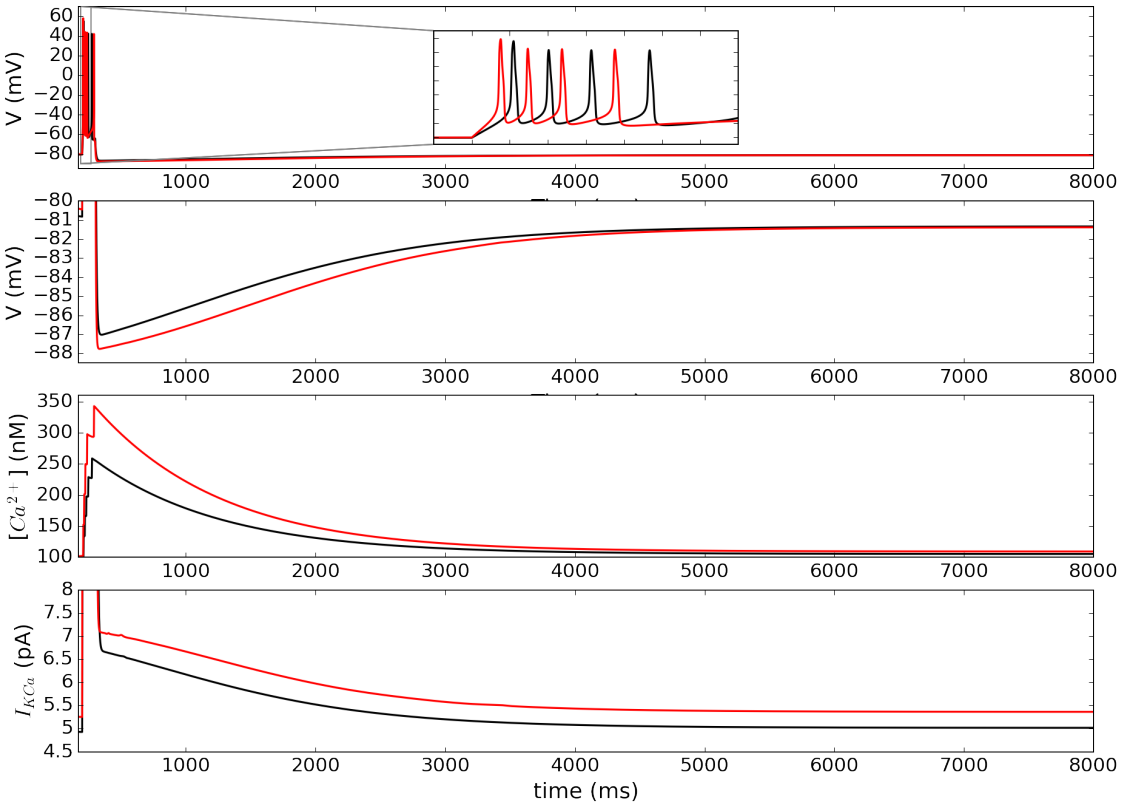


**Figure 3:** Responses of the yPC (black traces) and aPC (red traces) models to 100 ms pulse (top panel). Current amplitude adjusted to produce 5 spikes in each cell (yPC: 80 pA; aPC: 120 pA). Inset zooms in on the response to see the temporal relationship of spiking in the two cells. Second panel zooms in to better show the amplitude and time course of the AHP. The corresponding intracellular $Ca^{2+}$ concentration and SK currents for each cell can be seen in the third and fourth panels, respectively. Parameters for yPC: $A_{NaT}$ = 2.0, $A_{CaL}$ = 0.4, $A_{KaD}$ = 50.0, $A_{KaSK}$ = 1.3, $r_{KaD}$ = 1.0, $r_{Ca}$ = 1e$^{-3}$, $k_{Ca}$ = 8e$^{-6}$. All parameters for aPC the same except $A_{CaL}$ = 0.7.

## 3.3 Modeling age-related changes in burst firing

### 3.3.1 Bursting in response to stimulation

Some CA1 PCs fire bursts instead of trains of individual spikes, [38, 111–113], especially in certain developmental periods [114]. Burst firing can be generated in the model with several different parameter combinations. For the following simulations, we decreased the maximal amplitude and increased the activation time constant of the KD current, increased the maximal amplitude of the SK current, and made changes to the $Ca^{2+}$ handling, all within physiological limits. Under this parameter regime, model PCs are silent at rest but burst if stimulated (Fig. 4).

To explore the effects of aging on bursting, we fixed all parameters except for the maximum $Ca^{2+}$ current amplitude, as in previous simulations. We then stimulated the two model PCs with a series of square pulse current injections ranging from 20 to 145 pA to compare their responses. As mentioned previously, the larger $Ca^{2+}$ current in the aPC model causes them to fire sooner after stimulus onset than in the yPC model in all simulations. However, the relative timing of the two PCs' firing after the first burst depends on the stimulus amplitude.

At 20 pA, the aPC model bursts sooner but fires fewer spikes per burst than the yPC model. The aPC model then recovers before the yPC model and fires another burst towards the end of the stimulus, while yPC fires only one burst during the same period. At 45 pA, the initial bursts are almost coincident, but the larger AHP in aPC causes it to fire later than the yPC by the second burst. The aPC continues to fire later and with fewer spikes per burst than the yPC for the duration of the pulse. At 70 pA, the bursting in yPC and aPC is nearly coincident. While the aPC model has a larger AHP, it also fires fewer spikes per burst than the yPC model, allowing the two cells to recover and fire again at approximately the same time. At 95 pA, both cells now fire doublets, but the aPC model has a larger interspike interval and larger AHP, slowing its frequency of firing relative to the yPC model. The yPC fires 10 doublet bursts, while the aPC model fires only 7 in the same stimulation period. At the higher stimulation amplitudes (120 and 145 pA) the interspike interval in aPC becomes larger such that it eventually spikes tonically rather than bursting, while the yPC continues to fire doublets 4).

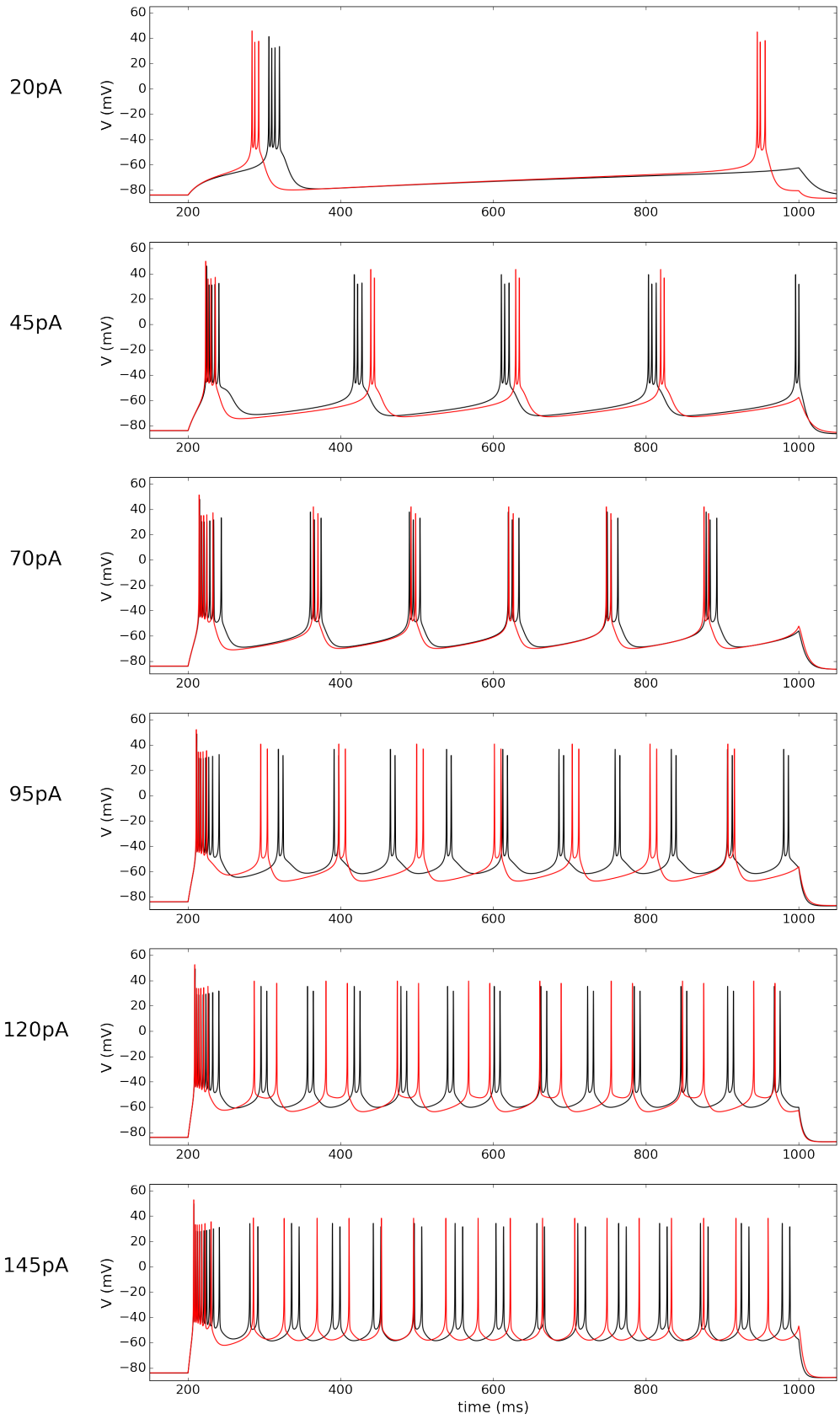


**Figure 4:** Bursting in the yPC (black traces) and aPC (red traces) models in response to 800 ms current injections of varying stimulus amplitudes (indicated to the left of each panel). Parameters for yPC: $A_{NaT}$ = 2.0, $A_{CaL}$ = 0.4, $A_{KaD}$ = 20.0, $A_{KaSK}$ = 2.5, $r_{KaD}$ = 2.5, $r_{Ca}$ = 5e$^{-3}$, $k_{Ca}$ = 6e$^{-6}$. All parameters for aPC the same except $A_{CaL}$ = 0.7.

### 3.3.2 Spontaneous bursting

A small percentage of CA1 PCs fire spontaneous bursts in the absence of any stimulation [112, 113, 115]. To generate spontaneous bursting in model neurons, we increased both the maximum amplitude of the $Na^+$ and KD currents, decreased both the maximum amplitude of the SK current and the time constant of activation for the KD current, and increased the removal rate for $Ca^{2+}$. Under this generic parameter regime, the yPC model fires spontaneous bursts at a frequency of $\sim$2 Hz with 3 spikes per burst (Fig. 5), similar to recordings [38].

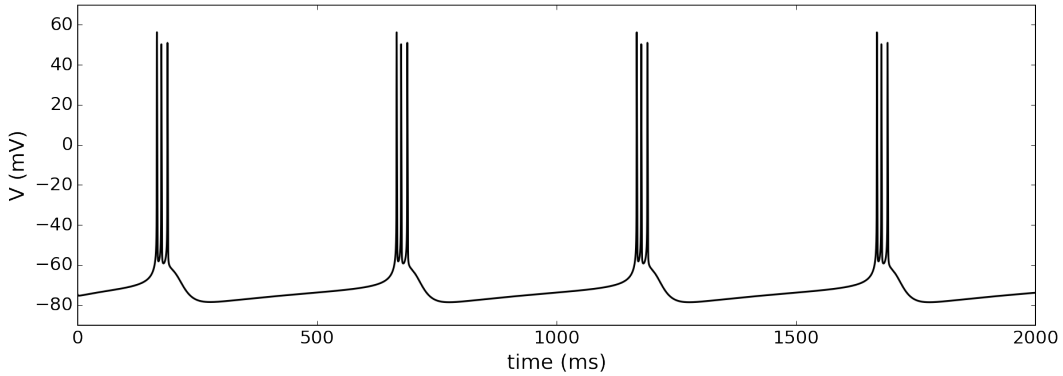


**Figure 5:** Spontaneous bursting in the yPC model. Parameters: $A_{NaT}$ = 4.0, $A_{CaL}$ = 0.4, $A_{KaD}$ = 30.0, $A_{KaSK}$ = 1.1, $r_{KaD}$ = 1.0, $r_{Ca}$ = 1e$^{-2}$, $k_{Ca}$ = 6e$^{-6}$, $I_F$ = 0.0.

Increasing the $Ca^{2+}$ channel density to simulate aging, as previously, changed the spontaneous bursting pattern (Fig. 6). The aPC model still fires regularly in the absence of stimulation, but fires 2 spikes instead of 3 per burst as in the yPC model. So while the $Ca^{2+}$ current is larger for the aPC model, the maximum accumulation of $Ca^{2+}$ is only $\sim$10 nM more than in the yPC. It is worth noticing that the quotient of the $Ca^{2+}$ current amplitude of the yPC with respect to aPC model is 4/7 (more than one half), which shows the nonlinear effects of the activation of the SK currents. There is a larger SK current in aPC due to the increased $Ca^{2+}$, but again, because yPC fires an additional time, the two cells end up reaching the same maximum current amplitude. In other words, the 'brake' on the two cells is roughly equal, and the larger $Ca^{2+}$ influx in the aPC model then means that it can burst at a higher frequency of $\sim$3 Hz.

## 3.4 Responses to local field potential forcing

Square pulse stimulation is useful and crucial for examining the timing of neural responses and also to calibrate the model so that the different currents yield responses like those observed experimentally. The resulting family of dynamical systems (same model, different parameters, in this case for the current amplitude). However, square pulse stimulation it is not a physiologically realistic stimulus. To simulate simulate local field potential (LFP) forcing onto CA1 PCs, we use an Ornstein-Uhlenbeck stochastic process [61, 62]. We began by stimulating PCs with parameters set to produce an adaptive firing pattern, as in Section 3.1. In the yPC model, LFP forcing produced repetitive, irregular firing at a frequency of $\sim$3Hz (Fig. 7, top panel). This firing pattern and frequency is similar to recordings of spontaneous firing in CA1 PCs [116, 117], particularly in response to specific brain rhythms recorded in the surrounding field [118–120].

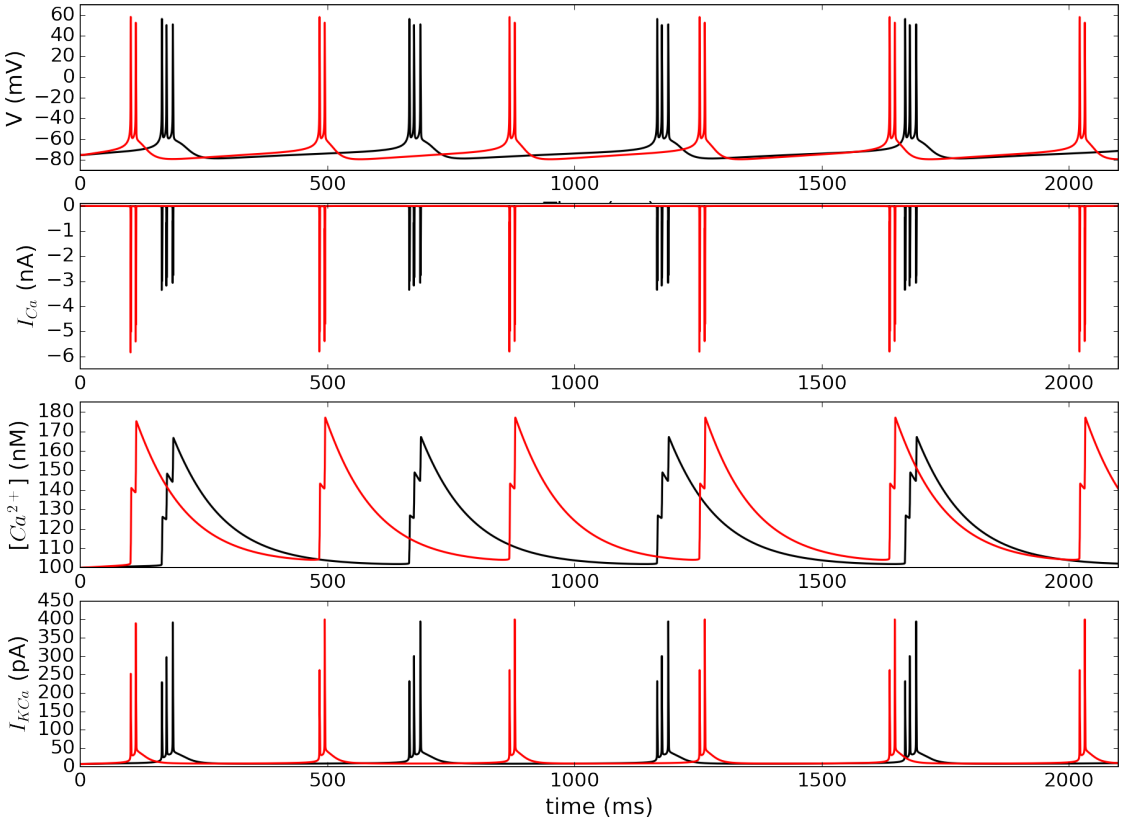


**Figure 6:** Comparison of spontaneous bursting in the yPC (black traces) versus aPC (red traces) model. Voltage responses are shown in the top panel. Corresponding $Ca^{2+}$ currents, intracellular $Ca^{2+}$ concentration, and SK currents for each cell can be seen in the second, third, and fourth panels, respectively. Parameters for yPC: same as in Fig. 5. All parameters for aPC the same except $A_{CaL}$ = 0.7.

The aPC model with increased $Ca^{2+}$ channel expression show a similar irregular firing pattern, but with a slower frequency (Fig. 7, second panel; also compare overlap in third panel). In a time window of 4 seconds, the yPC model fires 15 times, while the aPC fires about 10 times (2/3). In fact, the simulation shows several time points when the two cells fire almost simultaneously and then the yPC model fires again while the aged cell fails to do so. This apparent 'spike failure' has been observed in recordings of aged cells [19].

Next, we set the parameters to produce conditional bursting.[1] Under these conditions, LFP forcing in the yPC model produced irregular burst firing at a frequency of ∼5Hz (i.e., theta frequency) with a variable number of spikes (2-5) per burst (Fig. 8, top panel). This firing pattern is similar to spontaneous activity recorded in a subset of CA1 PCs known as phasic theta-ON cells, which preferentially burst during theta activity recorded from the surrounding field [118, 119, 121].

Increasing $Ca^{2+}$ channel expression in the aged model PC does not change the basic firing pattern (Fig. 8, middle panel). In response to LFP forcing, aged PCs still fire irregular bursts at

[1] We also stimulated model PCs with LFP forcing when parameters were set to produce spontaneous bursting. This produced firing similar to that recorded in animal models of epilepsy (citations?) This result is not shown here but can be reproduced in our Jupyter notebook.

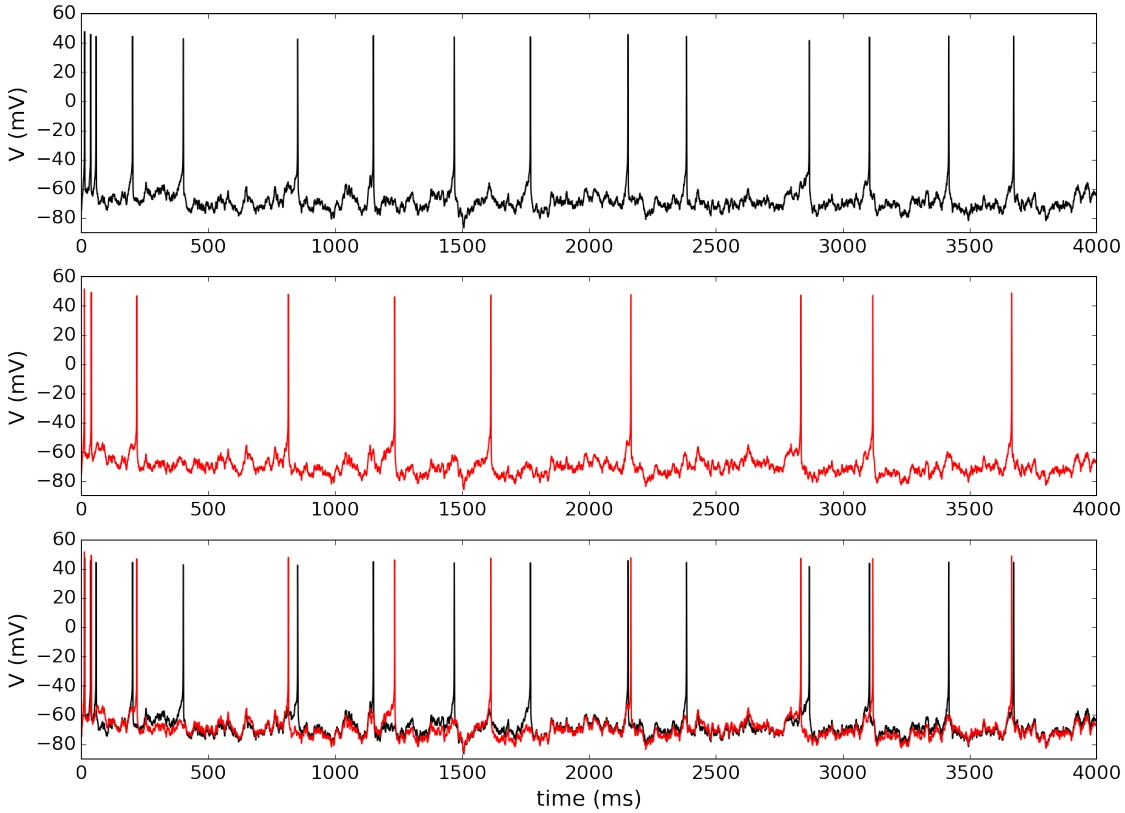


**Figure 7:** Responses of yPC (black traces) and aPC (red traces) models to LFP forcing. Top panel shows just the yPC response, second panel the aPC response, and the third panel shows the overlap of the two traces. Parameters for yPC and aPC models same as in Fig. 1. LFP parameters: $\mu_F$=-40.0 pA, $\sigma_F$=20.0 pA, $\tau_F$=1/2.0 for both models.

approximately the same frequency as in the yPC model ($\sim$5Hz, theta). However, the aPC model fires fewer spikes per burst (2-4), with a higher occurrence of 2-spike bursts. Also, the timing of the bursts in the aPC model is altered relative to the yPC model (see third panel overlap).

# 4 Discussion

## 4.1 Cellular heterogeneity

Here we show that a three-dimensional, single-compartment model derived from first principles of thermodynamics is capable of reproducing the diversity of firing patterns recorded in CA1 PCs. Moving between the different adaptive and bursting firing patterns was achieved primarily by changes to the relative expression of ion channels in the model. While we did not systematically explore the full parameter space, future work could include bifurcation analysis to determine the boundaries for each firing pattern. The flexibility of the model could be useful for researchers looking to understand the effects of PC heterogeneity on network function. Geiller and colleagues write, “Until very recently, hippocampus models and theories were built on a view of homogenous population of principal cells” [122]. However, studies have shown that there is substantial heterogeneity in the firing patterns of CA1 PCs, especially during different development stages (for review,

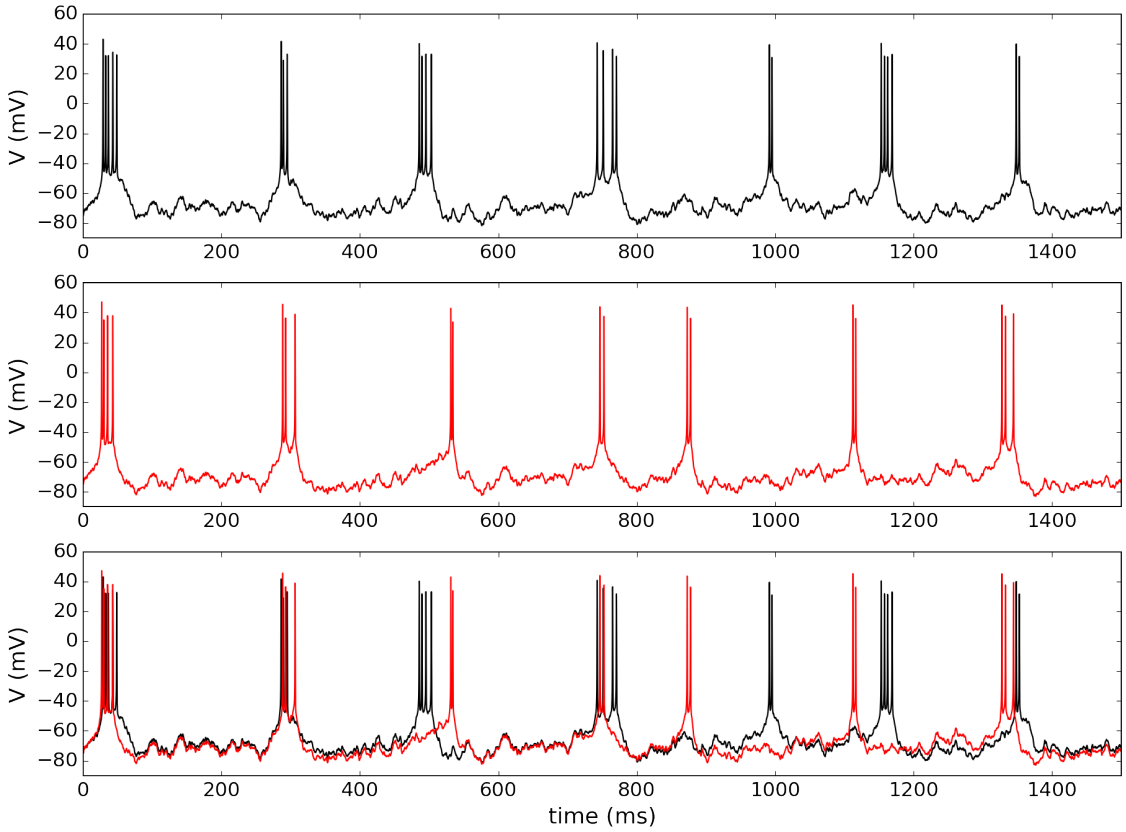


**Figure 8:** Responses of the yPC (black traces) and aPC (red traces) models to LFP forcing. Top panel shows just the yPC model response, second panel the aPC response, and the third panel shows the overlap of the two traces. Parameters for yPC and aPC models are the same as in Fig. 4. LFP parameters same as in Fig. 7.

see [47]). Lee and colleagues write, "how the heterogeneous PCs integrate into the CA1 circuit remains unknown" [123].

Experimentally, it is difficult to precisely quantify how many PCs in a given network are displaying a specific firing pattern, and even harder if not impossible to manipulate these percentages. Furthermore, cells can transition between firing patterns [124], meaning the percentages might fluctuate. With our minimal model, however, we could build small networks with different balances of adapting versus bursting PCs, for example, and explore how changing these balances affects network output. We could also model the progression of aging in the network by varying the percentage of PCs which have altered $Ca^{2+}$ channel density, or implement a whole spectrum of channel expression across the simulated network.

## 4.2 Aging and $Ca^{2+}$ channel expression

Our model can also reproduce several changes in electrical activity observed in aged CA1 PCs, including larger AHPs [16–20] and increased adaptation [23–25]. We show that an increase in the L-type $Ca^{2+}$ current amplitude to a level similar to that recorded in aged PCs is sufficient to reproduce the characteristic changes in cellular excitability associated with aging. The L-type

channel in our study was modeled after the $Ca_v1.2$ isoform based on work which implicates this channel as the primary contributor in rodent brain, responsible for ∼70-80% of the L-type current [64, 125]. mRNA expression of *Cacnac1C* (the gene encoding $Ca_v1.2$) is increased in aged mice and rats [29, 126]. Increases in plasma membrane expression [33] and phosphorylation [127] of $Ca_v1.2$ channels, both of which could lead to an increase in the number of 'functionally available' channels, have also been observed in aged rats. In addition, changes in *Cacna1c*/$Ca_v1.2$ expression are correlated with memory impairments [126, 128].

However, CA1 PCs also express the $Ca_v1.3$ isoform [129], which is responsible for ∼20% of the total L-type current [64, 125]. Studies have found both increased mRNA [29] and protein [31] expression of $Ca_v1.3$ in aged rats, and this increased expression is correlated with memory impairment [32]. Knockout studies in mice indicate it is this isoform, and not $Ca_v1.2$, which contributes to slow AHP generation [130], possibly via activation of colocalized SK channels [129]. While experimental studies have been complicated by a lack of pharmacological agents which can isolate currents carried by the different isoforms, it would be relatively simple with our model to study the contributions of these two channels. The primary difference between the two is a shift in the activation curve of the $Ca_v1.3$ channel to more hyperpolarized values, relative to $Ca_v1.2$ (around -20mV versus +3mV, respectively) [84]. In the model, changing the parameter $v_x$ would allow us to represent the different isoforms to explore how changes in the expression of each during aging might affect PC excitability.

Of course, there are many cellular changes apart from $Ca^{2+}$ channel expression that occur during aging and could contribute to altered electrical activity. For example, several studies have implicated $Ca^{2+}$ release from intracellular stores as an important contributor, particularly to larger AHPs in aged animals [23, 106] (for reviews see [131, 132]). We did not explore the role of intracellular $Ca^{2+}$ stores in this study ... emckhow to close here?

## 4.3 Aging and excitability

Our simulations do show changes in the electrical activity of aged PCs, but do these changes represent decreased excitability? This question relates more broadly to how we define excitability – the term is rarely clearly defined or used in a standardized way. In some studies, excitability is used to refer to change in firing rate of a cell over the course of an injected current pulse, claiming that PCs with stronger adaptation are less excitable (e.g., [24, 133]). In our simulations under the adaptive firing parameter regime, the aPC model did have stronger adaptation and fired fewer times during the stimulation period than the yPC model. However, this was only after the aPC model cell initially fired faster than the yPC model (compare the first 20ms of the responses in Fig. 2). Should we consider this decreased excitability?

If what concerns us is the activity of the cell over a given stimulation period, then the simulations under the bursting parameter regime are even less clear. The aPC model always fired fewer APs per burst than the yPC model, indicating something akin to stronger adaptation. However, if the 'event' we are considering is instead the burst, there are conditions under which aged model PCs fired a greater number of bursts in a given time period than young PCs (see for example Fig. 4, first panel and Fig. 8). How should we interpret these results with respect to excitability? To our knowledge, there are not many experimental studies to date have compared burst firing in young

versus aged animal PCs, perhaps because of the relatively low percentage of cells with this firing pattern in certain developmental periods. In an in vivo study comparing interspike intervals from freely behaving rats in rest and during running activity [134], no significant difference in mean firing rate for young and old animals. In more detail, the insterspike interval histograms for the pyramidal cells from both the young and the old animal cells were bimodal, with short intervals corresponding to spikes within burst and longer intervals for frequency adaptation or between burst spikes. During large irregular activity, an old rat had a larger percentage of ISIs in the 3âĂŞ7 ms, in comparison to a younger rat in the same study. The longer interspike intervals were similar but the younger rat showed a tendency toward displaying more spikes, on average, both in the sorter and larger interspike interval ranges. The altered timing of burst firing in aged PCs may be important for things like phase locking with local brain rhythm. Network level compensations could also explain the apparent discrepancy between the mechanisms and effects of increased $Ca^{2+}$currents explained here, and the lack of difference in the interspike intervals from the report by **(author?)**.

[emck]theta rhythm stuff here?

In other studies, researchers use excitability to refer to how easy it is to get a cell to fire in response to stimulation. For example, Daouda and colleagues write, “Excitability can be defined as a propensity of the neuron to generate, beyond a certain threshold, an output signal – the action potential (AP) – from a given input signal...” [135]. Similarly, Konstantinović and Filipović write, “Neuronal excitability can be defined...as the readiness of a nerve cell or a neural circuit to respond to a stimulus” [136]. In this context, excitability could be measured by the rheobase, or minimum current which generates firing in a neuron, as done in some studies of aging in CA1 (e.g., [137]). However, ‘propensity’ or ‘readiness’ could also be interpreted as how quickly a cell fires after stimulus onset.

In the AHP simulations, we saw that the aPC model required 40 pA of additional current to fire the same number of spikes as for the yPC model. [emck]do aged cells actually have higher rheobase? Yes, I think so. On the other hand, in all our simulations, the aPC model fired sooner than the yPC model and with larger amplitude APs in response to the same stimulus. These effects were a result of the increased $Ca^{2+}$ channel density in aged cells – the larger $Ca^{2+}$ current depolarized the cells faster and caused them to fire sooner, but it also caused the $Ca^{2+}$-dependent SK current to be larger and consequently slowed firing. It is as if the PCs were initially more excitable, but then ‘burned out’ more quickly than younger cells. [emck]also not sure how to close here.

# Funding

This work was supported by DGAPA-UNAM-PAPIIT IA208618 and IN228820, and DGAPA-UNAM-PAPIME PE114919 awarded to MAH-V. This work was also supported by DGAPA-UNAM-PAPIIT IA209817 awarded to ECM.

# References

[1] M.M. Oh, F.A. Oliveira, and J.F. Disterhoft. Learning and aging related changes in intrinsic neuronal excitability. Frontiers in Aging Neuroscience, 2:2, 2010.

[2] V. Rizzo, J. Richman, and S.V. Puthanveettil. Dissecting mechanisms of brain aging by studying the intrinsic excitability of neurons. Frontiers in Aging Neuroscience, 6:337, 2015.

[3] E.S. Rosenzweig and C.A. Barnes. Impact of aging on hippocampal function: plasticity, network dynamics, and cognition. Progress in Neurobiology, 69(3):143–179, 2003.

[4] C.A. Barnes. Memory deficits associated with senescence: a neurophysiological and behavioral study in the rat. Journal of Comparative and Physiological Psychology, 93(1):74, 1979.

[5] C.A. Barnes and B.L. McNaughton. An age comparison of the rates of acquisition and forgetting of spatial information in relation to long-term enhancement of hippocampal synapses. Behavioral Neuroscience, 99(6):1040, 1985.

[6] C.A. Barnes, G. Rao, and J. Shen. Age-related decrease in the N-methyl-D-aspartate R-mediated excitatory postsynaptic potential in hippocampal region CA1. Neurobiology of Aging, 18(4):445–452, 1997.

[7] F.H. Gage, S.B. Dunnett, and A. Björklund. Spatial learning and motor deficits in aged rats. Neurobiology of Aging, 5(1):43–48, 1984.

[8] C.A. Barnes and B.L. McNaughton. Spatial memory and hippocampal synaptic plasticity in senescent and middle-aged rats. The Psychobiology of Aging: Problems and Perspectives, pages 253–272, 1980.

[9] A. Caprioli, O. Ghirardi, A. Giuliani, M.T. Ramacci, and L. Angelucci. Spatial learning and memory in the radial maze: A longitudinal study in rats from 4 to 25 months of age. Neurobiology of Aging, 12(5):605–607, 1991.

[10] M.C. Newman and A.W. Kaszniak. Spatial memory and aging: Performance on a human analog of the morris water maze. Aging, Neuropsychology, and Cognition, 7(2):86–93, 2000.

[11] S.M. Wilkniss, M.G. Jones, D.L. Korol, P.E. Gold, and C.A. Manning. Age-related differences in an ecologically based study of route learning. Psychology and Aging, 12(2):372, 1997.

[12] D.L. Deupree, J. Bradley, and D.A. Turner. Age-related alterations in potentiation in the CA1 region in F344 rats. Neurobiology of Aging, 14(3):249–258, 1993.

[13] Ephron S Rosenzweig, Geeta Rao, Bruce L McNaughton, and Carol A Barnes. Role of temporal summation in age-related long-term potentiation–induction deficits. Hippocampus, 7(5):549–558, 1997.

[14] P.W. Landfield and G. Lynch. Impaired monosynaptic potentiation in in vitro hippocampal slices from aged, memory-deficient rats. Journal of Gerontology, 32(5):523–533, 1977.

[15] P.W. Landfield, J.L. McGaugh, and G. Lynch. Impaired synaptic potentiation processes in the hippocampus of aged, memory-deficient rats. Brain Research, 150(1):85–101, 1978.

[16] A. Kumar and T.C. Foster. 17$\beta$-estradiol benzoate decreases the AHP amplitude in CA1 pyramidal neurons. Journal of Neurophysiology, 88(2):621–626, 2002.

[17] A. Kumar and T. Foster. Environmental enrichment decreases the afterhyperpolarization in senescent rats. Brain Research, 1130:103–107, 2007.

[18] P.W. Landfield and T.A. Pitler. Prolonged $Ca^{2+}$-dependent afterhyperpolarizations in hippocampal neurons of aged rats. Science, 226(4678):1089–1092, 1984.

[19] J.C. Gant and O. Thibault. Action potential throughput in aged rat hippocampal neurons: regulation by selective forms of hyperpolarization. Neurobiology of Aging, 30(12):2053–2064, 2009.

[20] J.M. Power, W.W. Wu, E. Sametsky, M.M. Oh, and J.F. Disterhoft. Age-related enhancement of the slow outward calcium-activated potassium current in hippocampal CA1 pyramidal neurons in vitro. Journal of Neuroscience, 22(16):7234–7243, 2002.

[21] B.E. Alger and R.A. Nicoll. Epileptiform burst afterhyperolarization: Calcium-dependent potassium potential in hippocampal CA1 pyramidal cells. Science, 210(4474):1122–1124, 1980.

[22] J.R. Hotson and D.A. Prince. A calcium-activated hyperpolarization follows repetitive firing in hippocampal neurons. Journal of Neurophysiology, 43(2):409–419, 1980.

[23] J.C. Gant, M.M. Sama, P.W. Landfield, and O. Thibault. Early and simultaneous emergence of multiple hippocampal biomarkers of aging is mediated by $Ca^{2+}$-induced $Ca^{2+}$ release. Journal of Neuroscience, 26(13):3482–3490, 2006.

[24] J.R. Moyer, L.T. Thompson, J.P. Black, and J.F. Disterhoft. Nimodipine increases excitability of rabbit CA1 pyramidal neurons in an age-and concentration-dependent manner. Journal of Neurophysiology, 68(6):2100–2109, 1992.

[25] G.C. Tombaugh, W.B. Rowe, and G.M. Rose. The slow afterhyperpolarization in hippocampal CA1 neurons covaries with spatial learning ability in aged Fisher 344 rats. Journal of Neuroscience, 25(10):2609–2616, 2005.

[26] L.W. Campbell, S-Y. Hao, O. Thibault, E.M. Blalock, and P.W. Landfield. Aging changes in voltage-gated calcium currents in hippocampal CA1 neurons. Journal of Neuroscience, 16(19):6286–6295, 1996.

[27] M. Tanabe, B.H. Gähwiler, and U. Gerber. L-Type $Ca^{2+}$ channels mediate the slow $Ca^{2+}$-dependent afterhyperpolarization current in rat CA3 pyramidal cells in vitro. Journal of Neurophysiology, 80(5):2268–2273, 1998.

[28] O. Thibault, R. Hadley, and P.W. Landfield. Elevated postsynaptic $[Ca^{2+}]_i$ and L-type calcium channel activity in aged hippocampal neurons: Relationship to impaired synaptic plasticity. Journal of Neuroscience, 21(24):9744–9756, 2001.

[29] J.P. Herman, K-C. Chen, R. Booze, and P.W. Landfield. Up-regulation of $\alpha_{1D}$ $Ca^{2+}$ channel subunit mRNA expression in the hippocampus of aged F344 rats. Neurobiology of Aging, 19(6):581–587, 1998.

[30] O. Thibault and P.W. Landfield. Increase in single L-type calcium channels in hippocampal neurons during aging. Science, 272(5264):1017–1020, 1996.

[31] L.M. Veng and M.D. Browning. Regionally selective alterations in expression of the $\alpha_{1D}$ subunit ($Ca_v1.3$) of L-type calcium channels in the hippocampus of aged rats. Molecular Brain Research, 107(2):120–127, 2002.

[32] L.M. Veng, M.H. Mesches, and M.D. Browning. Age-related working memory impairment is correlated with increases in the L-type calcium channel protein $\alpha_{1D}$ ($Ca_v1.3$) in area CA1 of the hippocampus and both are ameliorated by chronic nimodipine treatment. Molecular Brain Research, 110(2):193–202, 2003.

[33] F.L. Núñez-Santana, M.M. Oh, M.D. Antion, A. Lee, J.W. Hell, and J.F. Disterhoft. Surface l-type $Ca^{2+}$ channel expression levels are increased in aged hippocampus. Aging Cell, 13(1):111–120, 2014.

[34] Christopher M Norris, Shelley Halpain, and Thomas C Foster. Reversal of age-related alterations in synaptic plasticity by blockade of L-type $Ca^{2+}$ channels. The Journal of Neuroscience, 18(9):3171–3179, 1998.

[35] M Sandin, Susan Jasmin, and TE Levere. Aging and cognition: facilitation of recent memory in aged nonhuman primates by nimodipine. Neurobiology of aging, 11(5):573–575, 1990.

[36] A Scriabine, T Schuurman, and J Traber. Pharmacological basis for the use of nimodipine in central nervous system disorders. The FASEB journal, 3(7):1799–1806, 1989.

[37] D. Bianchi, A. Marasco, A. Limongiello, C. Marchetti, H. Marie, B. Tirozzi, and M. Migliore. On the mechanisms underlying the depolarization block in the spiking dynamics of CA1 pyramidal neurons. Journal of Computational Neuroscience, 33(2):207–225, 2012.

[38] D. Golomb, C. Yue, and Y. Yaari. Contribution of persistent $Na^+$ current and M-type $K^+$ current to somatic bursting in CA1 pyramidal cells: combined experimental and modeling study. Journal of Neurophysiology, 96(4):1912–1926, 2006.

[39] N. Gu, K. Vervaeke, H. Hu, and J.F. Storm. Kv7/KCNQ/M and HCN/h, but not KCa2/SK channels, contribute to the somatic medium after-hyperpolarization and excitability control in CA1 hippocampal pyramidal cells. Journal of Physiology, 566(3):689–715, 2005.

[40] Panayiota Poirazi, Terrence Brannon, and Bartlett W Mel. Arithmetic of subthreshold synaptic summation in a model ca1 pyramidal cell. Neuron, 37(6):977–987, 2003.

[41] Mala M Shah, Michele Migliore, Ignacio Valencia, Edward C Cooper, and David A Brown. Functional significance of axonal kv7 channels in hippocampal pyramidal neurons. Proceedings of the National Academy of Sciences, 105(22):7869–7874, 2008.

[42] L-R. Shao, R. Halvorsrud, L. Borg-Graham, and J.F. Storm. The role of BK-type $Ca^{2+}$-dependent $K^+$ channels in spike broadening during repetitive firing in rat hippocampal pyramidal cells. Journal of Physiology, 521(1):135–146, 1999.

[43] Alan L Hodgkin and Andrew F Huxley. A quantitative description of membrane current and its application to conduction and excitation in nerve. The Journal of physiology, 117(4):500, 1952.

[44] M.A. Herrera-Valdez. A thermodynamic description for physiological transmembrane transport [version 2; peer review: 2 approved]. F1000Research, 7, 2018. https://doi.org/10.12688/f1000research.16169.2.

[45] M.A. Herrera-Valdez. Membranes with the same ion channel populations but different excitabilities. PloS one, 7(4):e34636, 2012.

[46] M.A. Herrera-Valdez, E.C. McKiernan, S.D. Berger, S. Ryglewski, C. Duch, and S. Crook. Relating ion channel expression, bifurcation structure, and diverse firing patterns in a model of an identified motor neuron. Journal of Computational Neuroscience, 34(2):211–229, 2013.

[47] E.C. McKiernan and D.F. Marrone. Ca1 pyramidal cells have diverse biophysical properties, affected by development, experience, and aging. PeerJ, 5:e3836, 2017.

[48] J.L. Hindmarsh and R.M. Rose. A model of neuronal bursting using three coupled first order differential equations. Proceedings of the Royal Society B, 221(1222):87–102, 1984.

[49] E. Av-Ron, H. Parnas, and L.A. Segel. A basic biophysical model for bursting neurons. Biological Cybernetics, 69(1):87–95, 1993.

[50] M.A. Herrera-Valdez. A simple derivation to describe the change in the transmembrane potential as a function of time without equivalent circuits. BiorXiv, 7, 2020. .

[51] B. Hille. Ion channels of excitable membranes. Sinauer Sunderland, MA, 2001.

[52] MI Kalinin and SA Kononogov. Boltzmann's constant, the energy meaning of temperature, and thermodynamic irreversibility. Measurement Techniques, 48(7):632–636, 2005.

[53] J. Rinzel. Excitation dynamics: insights from simplified membrane models. In Federation Proceedings, volume 44, pages 2944–2946. Federation of American Societies for Experimental Biology, 1985.

[54] E. Av-Ron, H. Parnas, and L. A. Segel. A minimal biophysical model for an excitable and oscillatory neuron. Biological Cybernetics, 65(6):487–500, 1991.

[55] M Covarrubias, A Wei, and L Salkoff. Shaker, Shal, Shab, and Shaw expresss independent K-current systems. Neuron(Cambridge, Mass.), 7(5):763–773, 1991.

[56] S. Tsunoda and L. Salkoff. The major delayed rectifier in both Drosophila neurons and muscle is encoded by Shab. Journal of Neuroscience, 15(7):5209–5221, 1995.

[57] Birgit Hirschberg, James Maylie, John P Adelman, and Neil V Marrion. Gating properties of single sk channels in hippocampal ca1 pyramidal neurons. Biophysical Journal, 77(4):1905–1913, 1999.

[58] Michael Rudolph and Alain Destexhe. Characterization of subthreshold voltage fluctuations in neuronal membranes. Neural Computation, 15(11):2577–2618, 2003.

[59] Daniel T Gillespie. The mathematics of brownian motion and johnson noise. American Journal of Physics, 64(3):225–239, 1996.

[60] Daniel T Gillespie. Exact numerical simulation of the Ornstein-Uhlenbeck process and its integral. Physical review E, 54(2):2084, 1996.

[61] Michael Rudolph, Zuzanna Piwkowska, Mathilde Badoual, Thierry Bal, and Alain Destexhe. A method to estimate synaptic conductances from membrane potential fluctuations. Journal of neurophysiology, 91(6):2884–2896, 2004.

[62] Alain Destexhe, Mathilde Badoual, Zuzanna Piwkowska, Thierry Bal, and Michael Rudolph. A novel method for characterizing synaptic noise in cortical neurons. Neurocomputing, 58:191–196, 2004.

[63] H. Murakoshi and J.S. Trimmer. Identification of the Kv2.1 $K^+$ channel as a major component of the delayed rectifier $K^+$ current in rat hippocampal neurons. Journal of Neuroscience, 19(5):1728–1735, 1999.

[64] J.W. Hell, R.E. Westenbroek, C. Warner, M.K. Ahlijanian, W. Prystay, M.M. Gilbert, T.P. Snutch, and W.A. Catterall. Identification and differential subcellular localization of the neuronal class C and class D L-type calcium channel $\alpha 1$ subunits. The Journal of Cell Biology, 123(4):949–962, 1993.

[65] M. Li, J.W. West, Y. Lai, T. Scheuer, and W.A. Catterall. Functional modulation of brain sodium channels by cAMP-dependent phosphorylation. Neuron, 8(6):1151–1159, 1992.

[66] D.A. Fadool and I.B. Levitan. Modulation of olfactory bulb neuron potassium current by tyrosine phosphorylation. Journal of Neuroscience, 18(16):6126–6137, 1998.

[67] J.B. Greer, M.C. Schmale, and L.A. Fieber. Whole-transcriptome changes in gene expression accompany aging of sensory neurons in Aplysia californica. BMC Genomics, 19(1):529, 2018.

[68] L. Groc, Z. Petanjek, B. Gustafsson, Y. Ben-Ari, E. Hanse, and R. Khazipov. In vivo blockade of neural activity alters dendritic development of neonatal ca1 pyramidal cells. European Journal of Neuroscience, 16(10):1931–1938, 2002.

[69] SOM Ketelaars, JA Gorter, EA Van Vliet, FH Lopes da Silva, and WJ Wadman. Sodium currents in isolated rat ca1 pyramidal and dentate granule neurones in the post-status epilepticus model of epilepsy. Neuroscience, 105(1):109–120, 2001.

[70] P. Sah, A.J. Gibb, and P.W. Gage. The sodium current underlying action potentials in guinea pig hippocampal CA1 neurons. The Journal of General Physiology, 91(3):373–398, 1988.

[71] Durga P Mohapatra, Hiroaki Misonou, Pan Sheng-Jun, Joshua E Held, D James Surmeier, and James S Trimmer. Regulation of intrinsic excitability in hippocampal neurons by activity-dependent modulation of the kv2. 1 potassium channel. Channels, 3(1):46–56, 2009.

[72] J. Scuvée-Moreau, A. Boland, A. Graulich, L. Van Overmeire, D. D'hoedt, F. Graulich-Lorge, E. Thomas, A. Abras, M. Stocker, J-F. Liégeois, and V. Seutin. Electrophysiological characterization of the sk channel blockers methyl-laudanosine and methyl-noscapine in cell lines and rat brain slices. British Journal of Pharmacology, 143(6):753–764, 2004.

[73] Kathryn S Richards, Kurt Bommert, Gabor Szabo, and Richard Miles. Differential expression of na+/k+-atpase $\alpha$-subunits in mouse hippocampal interneurones and pyramidal cells. The Journal of physiology, 585(2):491–505, 2007.

[74] D. Johnston and S. M-S. Wu. Foundations of Cellular Neurophysiology. MIT Press, 1995.

[75] L.P. Endresen, K. Hall, J.S. Høye, and J. Myrheim. A theory for the membrane potential of living cells. European Biophysics Journal, 29(2):90–103, 2000.

[76] P De Weer, David C Gadsby, and RF Rakowski. Voltage dependence of the na-k pump. Annual Review of Physiology, 50(1):225–241, 1988.

[77] M. Martina, J.H. Schultz, H. Ehmke, H. Monyer, and P. Jonas. Functional and molecular differences between voltage-gated K+ channels of fast-spiking interneurons and pyramidal neurons of rat hippocampus. Journal of Neuroscience, 18(20):8111–8125, 1998.

[78] W. Müller and K. Bittner. Differential oxidative modulation of voltage-dependent k+ currents in rat hippocampal neurons. Journal of Neurophysiology, 87(6):2990–2995, 2002.

[79] Marco Martina and Peter Jonas. Functional differences in na+ channel gating between fast-spiking interneurones and principal neurones of rat hippocampus. The Journal of Physiology, 505(3):593–603, 1997.

[80] A.R. Kay and R.K. Wong. Calcium current activation kinetics in isolated pyramidal neurones of the CA1 region of the mature guinea-pig hippocampus. The Journal of Physiology, 392:603, 1987.

[81] M. Estacion, A. Gasser, S.D. Dib-Hajj, and S.G. Waxman. A sodium channel mutation linked to epilepsy increases ramp and persistent current of $Na_v1.3$ and induces hyperexcitability in hippocampal neurons. Experimental Neurology, 224(2):362–368, 2010.

[82] S. Gasparini and J.C. Magee. Phosphorylation-dependent differences in the activation properties of distal and proximal dendritic Na+ channels in rat CA1 hippocampal neurons. The Journal of Physiology, 541(3):665–672, 2002.

[83] J.C. Magee and D. Johnston. Characterization of single voltage-gated na+ and ca2+ channels in apical dendrites of rat ca1 pyramidal neurons. The Journal of Physiology, 487(1):67, 1995.

[84] W. Xu and Diane Lipscombe. Neuronal $ca_v1.3$ $\alpha_1$ l-type channels activate at relatively hyperpolarized membrane potentials and are incompletely inhibited by dihydropyridines. Journal of Neuroscience, 21(16):5944–5951, 2001.

[85] B. Balasubramanian, J.P. Imredy, D. Kim, J. Penniman, A. Lagrutta, and J.J. Salata. Optimization of ca v 1.2 screening with an automated planar patch clamp platform. Journal of Pharmacological and Toxicological Methods, 59(2):62–72, 2009.

[86] B. Hirschberg, J. Maylie, J.P. Adelman, and N.V. Marrion. Gating of recombinant small-conductance ca-activated k+ channels by calcium. The Journal of General Physiology, 111(4):565–581, 1998.

[87] Âť alteration and restoration of k+ channel function by deletions at the n-and c-termini.

[88] M.M. Oh, F.A. Oliveira, J. Waters, and J.F. Disterhoft. Altered calcium metabolism in aging ca1 hippocampal pyramidal neurons. Journal of Neuroscience, 33(18):7905–7911, 2013.

[89] J.C. Magee, R.B. Avery, B.R. Christie, and D. Johnston. Dihydropyridine-sensitive, voltage-gated ca2+ channels contribute to the resting intracellular ca2+ concentration of hippocampal ca1 pyramidal neurons. Journal of Neurophysiology, 76(5):3460–3470, 1996.

[90] E. Jones, T. Oliphant, P. Peterson, et al. SciPy: Open source scientific tools for Python, 2001–. [Online; accessed April 2018].

[91] J.D. Hunter. Matplotlib: A 2d graphics environment. Computing In Science & Engineering, 9(3):90–95, 2007.

[92] D. Mondaca. pyprocess, 2012–.

[93] Fernando Pérez and Brian E. Granger. IPython: a system for interactive scientific computing. Computing in Science and Engineering, 9(3):21–29, May 2007.

[94] T. Kluyver, B. Ragan-Kelley, F. Pérez, B.E. Granger, M. Bussonnier, J. Frederic, K. Kelley, J.B. Hamrick, J. Grout, S. Corlay, P. Ivanov, D. Avila, S. Abdalla, C. Willing, and Jupyter Development Team. Jupyter Notebooks-a publishing format for reproducible computational workflows. In F. Loizides and B. Schmidt, editors, Positioning and Power in Academic Publishing: Players, Agents and Agendas, pages 87–90, 2016.

[95] K.C. Chen, E.M. Blalock, O. Thibault, P. Kaminker, and P.W. Landfield. Expression of $\alpha$1D subunit mRNA is correlated with L-type Ca2+ channel activity in single neurons of hippocampal "zipper" slices. Proceedings of the National Academy of Sciences, 97(8):4357–4362, 2000.

[96] D.V. Madison and R.A. Nicoll. Control of the repetitive discharge of rat CA1 pyramidal neurones in vitro. Journal of Physiology, 354(1):319–331, 1984.

[97] R.W. Stackman, R.S. Hammond, E. Linardatos, A. Gerlach, J. Maylie, J.P. Adelman, and T. Tzounopoulos. Small conductance Ca2+-activated K+ channels modulate synaptic plasticity and memory encoding. Journal of Neuroscience, 22(23):10163–10171, 2002.

[98] M. Borde, J.R. Cazalets, and W. Buno. Activity-dependent response depression in rat hippocampal CA1 pyramidal neurons in vitro. Journal of Neurophysiology, 74(4):1714–1729, 1995.

[99] N. Gu, H. Hu, K. Vervaeke, and J.F. Storm. SK (KCa2) channels do not control somatic excitability in CA1 pyramidal neurons but can be activated by dendritic excitatory synapses and regulate their impact. Journal of Neurophysiology, 100(5):2589–2604, 2008.

[100] S-C. Jung and D.A. Hoffman. Biphasic somatic A-type K+ channel downregulation mediates intrinsic plasticity in hippocampal CA1 pyramidal neurons. PLOS ONE, 4(8):e6549, 2009.

[101] J. Kim, D-S. Wei, and D.A. Hoffman. Kv4 potassium channel subunits control action potential repolarization and frequency-dependent broadening in rat hippocampal CA1 pyramidal neurones. Journal of Physiology, 569(1):41–57, 2005.

[102] R. Malik and S. Chattarji. Enhanced intrinsic excitability and EPSP-spike coupling accompany enriched environment-induced facilitation of LTP in hippocampal CA1 pyramidal neurons. Journal of Neurophysiology, 107(5):1366–1378, 2012.

[103] J.F. Disterhoft, L.T. Thompson, J.R. Moyer, and D.J. Mogul. Calcium-dependent afterhyperpolarization and learning in young and aging hippocampus. Life Sciences, 59(5):413–420, 1996.

[104] J.F. Storm. An after-hyperpolarization of medium duration in rat hippocampal pyramidal cells. Journal of Physiology, 409(1):171–190, 1989.

[105] J.F. Storm. Potassium currents in hippocampal pyramidal cells. Progress in Brain Research, 83:161–187, 1990.

[106] K. Bodhinathan, A. Kumar, and T.C. Foster. Redox sensitive calcium stores underlie enhanced after hyperpolarization of aged neurons: role for ryanodine receptor mediated calcium signaling. Journal of Neurophysiology, 104(5):2586–2593, 2010.

[107] E.M. Blalock, J.T. Phelps, T. Pancani, J.L. Searcy, K.L. Anderson, J.C. Gant, J. Popovic, M.G. Avdiushko, D.A. Cohen, K.-C. Chen, N.M. Porter, and O. Thibault. Effects of long-term pioglitazone treatment on peripheral and central markers of aging. PLOS ONE, 5(4):e10405, 2010.

[108] C.C. Kaczorowski and J.F. Disterhoft. Memory deficits are associated with impaired ability to modulate neuronal excitability in middle-aged mice. Learning & Memory, 16(6):362–366, 2009.

[109] E.A. Matthews, J.M. Linardakis, and J.F. Disterhoft. The fast and slow afterhyperpolarizations are differentially modulated in hippocampal neurons by aging and learning. Journal of Neuroscience, 29(15):4750–4755, 2009.

[110] C.C. Kaczorowski, J. Disterhoft, and N. Spruston. Stability and plasticity of intrinsic membrane properties in hippocampal ca1 pyramidal neurons: effects of internal anions. The Journal of Physiology, 578(3):799–818, 2007.

[111] R. Azouz, M.S. Jensen, and Y. Yaari. Ionic basis of spike after-depolarization and burst generation in adult rat hippocampal CA1 pyramidal cells. Journal of Physiology, 492(1):211–223, 1996.

[112] M.S. Jensen, R. Azouz, and Y. Yaari. Variant firing patterns in rat hippocampal pyramidal cells modulated by extracellular potassium. Journal of Neurophysiology, 71(3):831–839, 1994.

[113] H. Su, G. Alroy, E.D. Kirson, and Y. Yaari. Extracellular calcium modulates persistent sodium current-dependent burst-firing in hippocampal pyramidal neurons. Journal of Neuroscience, 21(12):4173–4182, 2001.

[114] S. Chen, C. Yue, and Y. Yaari. A transitional period of $Ca^{2+}$-dependent spike afterdepolarization and bursting in developing rat CA1 pyramidal cells. Journal of Physiology, 567(1):79–93, 2005.

[115] M.S. Jensen, R. Azouz, and Y. Yaari. Spike after-depolarization and burst generation in adult rat hippocampal CA1 pyramidal cells. Journal of Physiology, 492(1):199–210, 1996.

[116] F. Manseau and S. Williams. Tuning in the hippocampal theta band in vitro: methodologies for recording from the isolated rodent septohippocampal circuit. JoVE (Journal of Visualized Experiments), (126):e55851, 2017.

[117] Q. Yang, Y-D. Hu, X-F. Wang, and F-S. Zheng. Dl-3n-butylphthalide reduces epileptiform activity through GluA2-lacking calcium-permeable AMPARs in epilepsy models. Oncotarget, 8(58):98242, 2017.

[118] B.H. Bland, J. Konopacki, and R.H. Dyck. Relationship between membrane potential oscillations and rhythmic discharges in identified hippocampal theta-related cells. Journal of Neurophysiology, 88(6):3046–3066, 2002.

[119] B.H. Bland, J. Konopacki, and R. Dyck. Heterogeneity among hippocampal pyramidal neurons revealed by their relation to theta-band oscillation and synchrony. Experimental Neurology, 195(2):458–474, 2005.

[120] C.Y.L. Huh, B. Amilhon, K.A. Ferguson, F. Manseau, S.G. Torres-Platas, J.P. Peach, S. Scodras, N. Mechawar, F.K. Skinner, and S. Williams. Excitatory inputs determine phase-locking strength and spike-timing of CA1 stratum oriens/alveus parvalbumin and somatostatin interneurons during intrinsically generated hippocampal theta rhythm. Journal of Neuroscience, 36(25):6605–6622, 2016.

[121] L.V. Colom and B.H. Bland. State-dependent spike train dynamics of hippocampal formation neurons: evidence for theta-on and theta-off cells. Brain Research, 422(2):277–286, 1987.

[122] T. Geiller, S. Royer, and J-S. Choi. Segregated cell populations enable distinct parallel encoding within the radial axis of the ca1 pyramidal layer. Experimental Neurobiology, 26(1):1–10, 2017.

[123] S-H. Lee, I. Marchionni, M. Bezaire, C. Varga, N. Danielson, M. Lovett-Barron, A. Losonczy, and I. Soltesz. Parvalbumin-positive basket cells differentiate among hippocampal pyramidal cells. Neuron, 82(5):1129–1144, 2014.

[124] M. Steriade, I. Timofeev, N. Dürmüller, and F. Grenier. Dynamic properties of corticothalamic neurons and local cortical interneurons generating fast rhythmic (30–40 Hz) spike bursts. Journal of Neurophysiology, 79(1):483–490, 1998.

[125] M.J. Sinnegger-Brauns, A. Hetzenauer, I.G. Huber, E. Renström, G. Wietzorrek, S. Berjukov, M. Cavalli, D. Walter, A. Koschak, R. Waldschütz, S. Herin, S. Bova, P. Rorsman, O. Pongs, N. Singewald, and J. Striessnig. Isoform-specific regulation of mood behavior and pancreatic $\beta$ cell and cardiovascular function by L-type $Ca^{2+}$ channels. The Journal of Clinical Investigation, 113(10):1430–1439, 2004.

[126] P. Zanos, S. Bhat, C.E. Terrillion, R.J. Smith, L.H. Tonelli, and T.D. Gould. Sex-dependent modulation of age-related cognitive decline by the L-type calcium channel gene Cacna1c ($Ca_v1.2$). European Journal of Neuroscience, 42(8):2499–2507, 2015.

[127] M.A. Davare and J.W. Hell. Increased phosphorylation of the neuronal L-type $Ca^{2+}$ channel $Ca_v1.2$ during aging. Proceedings of the National Academy of Sciences, 100(26):16018–16023, 2003.

[128] S. Moosmang, N. Haider, N. Klugbauer, H. Adelsberger, N. Langwieser, J. Müller, M. Stiess, E. Marais, V. Schulla, L. Lacinova, S. Goebbels, K.A. Nave, D.R. Storm, F. Hofmann, and T. Kleppisch. Role of hippocampal $Ca_v1.2$ $Ca^{2+}$ channels in NMDA receptor-independent synaptic plasticity and spatial memory. Journal of Neuroscience, 25(43):9883–9892, 2005.

[129] S.E.H. Bowden, S. Fletcher, D.J. Loane, and N.V. Marrion. Somatic colocalization of rat SK1 and D class ($Ca_v1.2$) L-type calcium channels in rat CA1 hippocampal pyramidal neurons. Journal of Neuroscience, 21(20):RC175–RC175, 2001.

[130] A.E. Gamelli, B.C. McKinney, J.A. White, and G.G. Murphy. Deletion of the L-type calcium channel $Ca_v1.3$ but not $Ca_v1.2$ results in a diminished sAHP in mouse CA1 pyramidal neurons. Hippocampus, 21(2):133–141, 2011.

[131] O. Thibault, J.C. Gant, and P.W. Landfield. Expansion of the calcium hypothesis of brain aging and Alzheimer's disease: minding the store. Aging Cell, 6(3):307–317, 2007.

[132] E.C. Toescu and M. Vreugdenhil. Calcium and normal brain ageing. Cell Calcium, 47(2):158–164, 2010.

[133] M.M. Oh, J.M. Power, L.T. Thompson, P.L. Moriearty, and J.F. Disterhoft. Metrifonate increases neuronal excitability in CA1 pyramidal neurons from both young and aging rabbit hippocampus. Journal of Neuroscience, 19(5):1814–1823, 1999.

[134] Anne C Smith, Jason L Gerrard, Carol A Barnes, and Bruce L McNaughton. Effect of age on burst firing characteristics of rat hippocampal pyramidal cells. Neuroreport, 11(17):3865–3871, 2000.

[135] G. Daoudal and D. Debanne. Long-term plasticity of intrinsic excitability: learning rules and mechanisms. Learning & Memory, 10(6):456–465, 2003.

[136] L.M. Konstantinović and S.R. Filipović. Effects of near-infrared low-level laser stimulation on neuronal excitability. In Photobiomodulation in the Brain, pages 233–240. Elsevier, 2019.

[137] B. Potier, Y. Lamour, and P. Dutar. Age-related alterations in the properties of hippocampal pyramidal neurons among rat strains. Neurobiology of Aging, 14(1):17–25, 1993.